Construction and Building Materials 411 (2024) 134310

Contents lists available at ScienceDirect

Construction and Building Materials

journal homepage: www.elsevier.com/locate/conbuildmat

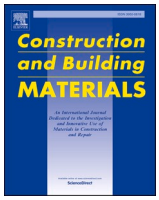

Exploring the short-term water damage characteristics of asphalt mixtures: The combined effect of salt erosion and dynamic water scouring

Mingjun Guo [a], Tengfei Nian [b,*], Ping Li [b], Viktor Pavlovich Kovalskiy [a]

[a] Faculty of Civil Engineering, Thermal Power Engineering and Gas Supply, Vinnytsia National Technical University, Voiniv-Internatsionalistiv St, 7, Vinnytsia, Vinnytsia Oblast 21000, Ukraine
[b] School of Civil Engineering, Lanzhou University of Technology, Lanzhou 730050, Gansu, China

ARTICLE INFO

Keywords:
Road engineering
Asphalt mixture
Dynamic water scouring
Deicing salt
Water damage

ABSTRACT

In icy or snowy conditions, improper application and uneven dispersion of deicing salts on roadways can lead to saltwater accumulation, subsequently causing roadway scouring when vehicles transit. This study aims to assess the combined influence of salt erosion and dynamic water scouring on short-term water damage of asphalt mixtures. A custom-designed dynamic water scouring simulation apparatus is used, employing three diverse deicing salt solutions as agents for dynamic water scouring. Numerous iterations of dynamic water scouring tests are conducted on two types of graded asphalt mixtures. Post-scouring, alterations in air void content and water stability are evaluated through void content tests, Marshall water immersion tests, and freeze-thaw splitting tests. Additionally, the GM (1,N) damage prediction model from gray theory is applied for data modeling and prediction. The results reveal a significant impact of the combined effects of salt erosion and dynamic water scouring on the short-term performance of asphalt mixtures. In the early phase, dynamic water scouring primarily influences the asphalt composite, augmenting micro-cracks and causing aggregate disintegration. The intermediate phase sees the disintegration of the asphalt membrane by deicing salts, disrupting adhesion between asphalt and aggregate, and progressively leading to the emergence of new micro-cracks. During later stages, dynamic water scouring continues to deteriorate the asphalt composite, building on the erosion instigated by deicing salts, resulting in the expansion of newly formed micro-cracks and further aggregate disintegration. Among the three deicing salts, CH_4N_2O exhibits the most pronounced impact on short-term water damage, followed by NaCl, while CH_2CH_3OH has the least effect. Increasing the fine aggregate proportion in the asphalt mixture enhances water damage resistance. The GM (1,N) damage prediction model effectively anticipates air void content and water stability of asphalt mixtures. The research outcomes offer theoretical and technical support for understanding the durability and service lifespan of asphalt pavements in cold regions.

1. Introduction

Road infrastructure has a crucial role in contemporary society, characterized by the widespread use of asphalt pavements globally. However, with the continuous growth in traffic density and the increasing loads borne by vehicles, the challenge of highway maintenance and administration faces an unprecedented level of complexity[1,2]. Notably, the materials that constitute pavement are subjected to various environmental stressors, such as water-induced erosion, freeze-thaw cycles in cold environments, and chemical immersion. These factors collectively exacerbate the rate of pavement degradation [3,4].

The presence of water on roadway surfaces can lead to specific interactions, particularly when vehicles are moving at high speeds. This can result in the formation of cavities between the tire tread and the pavement. The size of these cavities depends on the properties of the tire tread pattern and the structural composition of the road surface.

When the tire tread pattern comes into contact with the roadway, the water within these cavities undergoes rapid compression, forcing it into any existing gaps or fissures. As the tire continues to roll, the compressed water creates a positive high-pressure stream that can erode the asphalt film or any superficial fractures. Upon disengagement of the tire tread from the surface, a vacuum forms within the cavity, pulling the compacted water from the interior of the asphalt pavement. This generates a

* Corresponding author.
E-mail address: tengfeinian@lut.edu.cn (T. Nian).

https://doi.org/10.1016/j.conbuildmat.2023.134310
Received 8 July 2023; Received in revised form 20 November 2023; Accepted 22 November 2023
Available online 30 November 2023

negative high-pressure water flow that persists in eroding surface fissures.

This dynamic water-scouring effect has a detrimental impact on the adhesive strength and internal cohesion of the asphalt composite. It leads to the peeling of the asphalt film and the expansion of fractures in the pavement, compromising its integrity[5,6].

Several scholars have investigated the impact of dynamic water scouring on roads. Gao et al.[7] performed field tests to determine dynamic water pressure values on asphalt surfaces at varying vehicular speeds, thereby establishing a correlation between dynamic water pressure and vehicle speed. Zhang et al.[8], through simulation, revealed that in asphalt composites subjected to dynamic water erosion, the positive pressure peak within the voids is approximately 1–2 times the negative pressure peak. Li et al.[9] argue that dynamic water erosion significantly affects the stability of the skeletal structure of asphalt composites. Guo et al.[10], using indoor simulations of dynamic water erosion on asphalt pavements under various road conditions, propose that water temperature has a crucial role in influencing the resistance of asphalt pavements to dynamic water erosion. According to their findings, there is an inverse relationship between an increase in water temperature and the resilience of asphalt pavements to dynamic water erosion.

Deicing salts are often employed in roadway deicing operations to mitigate the impact of ice and snow[11,12]. However, improper application or uneven distribution of deicing agents can result in the partial thawing of icy and snowy surfaces, leaving other areas frozen and creating "ice and snow gullies." These gullies hinder the flow of thawed ice and snow to the roadside, causing the accumulation of "saltwater" on the roadway surface for extended periods during snowy conditions. As vehicles travel through these areas, the high-speed wash from the saltwater can have detrimental effects on the roadway material [13–15]. Xiong et al.[16,17] conducted a thorough examination of the erosion and performance degradation of asphalt mixtures when subjected to sodium chloride and sulfate. They used a custom-engineered dynamic water-salt erosion apparatus for their experiments. The team primarily employed the splitting test to evaluate the influence of different concentration levels of individual salts, namely sodium chloride and sodium sulfate, on the performance characteristics of asphalt mixtures. Advanced analytical techniques, including the gray entropy method and multiple linear regression analysis, were applied to determine the relative importance of each determinant factor in the erosion process.

Still, there is limited research addressing the short-term water damage of asphalt mixtures caused by the simultaneous impact of dynamic water scouring and deicing salt erosion. Among the various evaluative methods for assessing water-induced damage in asphalt mixtures, several tests are notable. The void content test, in particular, provides precise quantification of internal structural erosion resulting from water and chemical interactions[18]. The Marshall water immersion test serves as a metric for evaluating the stability and durability of materials under diverse aqueous conditions. Additionally, the freeze-thaw splitting test replicates the cyclical freezing and thawing conditions experienced by asphalt mixtures in extreme winter climates. This test enables an assessment of material durability and water stability under such challenging environmental conditions[19].

In this study, a custom-designed dynamic water-scouring simulation apparatus is used to test two distinct asphalt mixtures and three individual deicing salt solutions. The research comprehensively assesses the impact of various deicing salt solutions and different instances of dynamic water scouring on short-term water damage to asphalt mixtures. The evaluation is conducted through the void content test, the Marshall water immersion test, and the freeze-thaw splitting test.

The present study used the gray system theory to navigate scenarios marked by limited data and deficient information. Introduced by Deng Julong in 1982, the theory provides a distinctive analytical approach to dealing with uncertainty in complex systems. The gray system theory offers a valuable framework for analyzing situations where data is limited and information is lacking, allowing for a more comprehensive understanding of complex and uncertain scenarios[20]. It focuses primarily on systems with sparse samples and restricted information, where information is partially known. The theory's main purpose is to create and expand the known segments of information to extract valuable insights. This methodology is well-suited for depicting and efficiently monitoring the operational behaviors and evolution patterns of systems. Therefore, the theory serves as an effective mathematical approach for resolving uncertainty problems arising from scarce data and insufficient information [21,22]. Among the various tools within the gray system theory, the GM (1,N) prediction model finds extensive application in areas such as logistics, agriculture, and cartography. However, its use in the study of road materials has been notably underreported. Consequently, this study proposes the use of the GM (1, N) predictive model to forecast and scrutinize the variation trends of air void content and water stability. This approach aims to provide both theoretical and technical foundations for ensuring the prolonged durability of asphalt pavements in cold regions.

2. Test materials and mix design

2.1. Asphalt

The asphalt incorporated in the research was KL-90 petroleum asphalt, intended for roadway application, with all pertinent technical indices adhering to existing standards upon evaluation. The technical indices are delineated in Table 1.

2.2. Aggregate and mineral filler

The coarse aggregate, fine aggregate, and mineral filler used in this research were obtained exclusively from the Wangjiaping Material Yard in Lanzhou City, Gansu Province. All relevant technical measures adhered to existing standards after thorough evaluation. The detailed technical measures are outlined in Tables 2–4.

2.3. Deicing salt

To elucidate the mechanistic effects of various deicing salts on the short-term water damage of asphalt mixtures, this study selected urea (CH_4N_2O), sodium chloride (NaCl), and ethanol (CH_2CH_3OH) as test subjects. These compounds were chosen due to their widespread use in winter road deicing and snow removal procedures, making the study's findings more representative of real-world scenarios. Sodium chloride is commonly used in winter road maintenance for its effective and cost-efficient snow-melting capabilities. Urea, a non-salt organic compound with extensive agricultural applications, is also utilized in winter road maintenance. Despite its lower efficacy in freezing point depression compared to sodium chloride, urea's low environmental impact and plant-absorbent properties make it a preferred choice in environmentally sensitive regions. Ethanol, representing alcohol-based snow melt agents, has a low freezing point and high volatility, allowing it to simulate harsh winter environmental conditions.

In the initial phase of the study, the research team conducted

Table 1
Technical indexes of asphalt.

Index	Test result	Requirement
Penetration (25 ℃, 100 g .5 s)/0.1 mm	88	80–100
Extensibility (15 ℃)/cm	> 100	≥ 100
Penetration Index	-1.1	-1.5~+ 1.0
Softening Point/℃	48.0	≥ 45
Density (15 ℃)/(g·cm^{-3})	1.033	—
Flash Point/℃	300	≥ 245
Dynamic viscosity (60 ℃)/Pa•s	151	≥ 140
Solubility/%	99.8	≥ 99.5

Table 2
Technical indicators of coarse aggregate.

Index	Test Result	Requirement
Crushed Stone Value/%	17.9	≤ 28
Solmdness/%	10.9	≤ 12
Apparent Particle Density	2.81	≥ 2.5
Los Angeles Abrasion Loss/%	17.2	≤ 30
Water Absorption/%	1.5	≤ 3

Table 3
Technical indicators of fine aggregate.

Index	Test Result	Requirement
Solmdness/%	9.1	≤ 12
Sand Equivalent/%	76	≥ 60
Apparent Particle Density	2.73	≥ 2.50
Mud Content/%	2.0	≤ 3

Table 4
Technical indicators of mineral filler.

Index	Test result	Requirement
Water Absorption/%	0.89	≤ 1
Hydrophilic Coefficient/%	≤ 1	≤ 1
Density/(t·m^{-3})	2.82	≥ 2.5
Appearance	No agglomerates	No agglomerates

freezing point tests on seven commonly utilized deicing salts at various concentrations [23]. The obtained data revealed a negligible disparity in freezing points within the range of 15% and 20% for CH_4N_2O. Conversely, a substantial difference was observed in freezing points when comparing concentrations of 15% and 20% for both NaCl and CH_2CH_3OH. Based on these findings, and considering both snow melting performance and economic viability, the research team selected 15% CH_4N_2O, 20% NaCl, and 20% CH_2CH_3OH as the deicing salt solutions for the experimental phase.

The deicing salts employed in this investigation include urea, characterized by a nitrogen content of ≥ 46.4 %, manufactured by Gansu Liu Chemical (Group) Co., Ltd.; industrial salt, with a sodium chloride content of ≥ 99.1 %, produced by Golmud Baojin Chemical Trade Co., Ltd.; and anhydrous ethanol, featuring an ethanol content of ≥ 99.7 %, fabricated by Tianjin Beichen Fangzheng Reagent Factory.

2.4. Mix design

The asphalt mixtures selected for the investigation are AC-13 and AC-16, and their corresponding aggregate gradations are illustrated in Figs. 1–2. The optimal asphalt-aggregate ratios, established through the Marshall compaction test, were found to be 5.1 % for AC-13 % and 4.5 % for AC-16. The maximal theoretical densities were identified as 2465 kg/m^3 and 2573 kg/m^3 for AC-13 and AC-16, respectively.

3. Experimental and theoretical analysis methods

3.1. Custom-designed dynamic water scouring simulation apparatus

The experiment used a dynamically designed and fabricated water-scouring simulation apparatus created by the research team to replicate the process of multiple dynamic water scours. This apparatus autonomously adjusts the gas pressure within its cavity to simulate the dynamic scouring and erosion induced by vehicular loads on authentic asphalt road surfaces. Capable of executing swift forward pressurization and reverse vacuum cycles, the dynamic water scouring simulator dynamically substitutes the pore water pressure within the specimen by modifying the atmospheric pressure on the specimen's surface, simulating the process of pore water dynamically eroding the asphalt mixture. As illustrated in Fig. 3, the dynamic water scouring simulation apparatus comprises a pressure vessel, test specimens, a pressure simulation system, and a computer control system. The pressure vessel, constructed from corrosion-resistant SUS316 stainless steel with high-pressure and high-temperature tolerance, has internal dimensions of 102 mm in diameter and 100 mm in height. The computerized control system is tripartite, consisting of a power supply subsystem, a protective mechanism, and a control encoder. The power supply governs the activation and deactivation of both the pressure apparatus and its corresponding solenoid valves, while the protective device ensures overload safeguarding for the entire test circuitry. The control encoder facilitates the customization of test parameters, including cycle frequency, duration, and intervals. The air compressor's maximum adjustable pressure is set at 0.75 MPa with an exhaust capacity of 0.4 m^3/min, powered by a 4 kW/5.5 P motor. The vacuum pump features a maximal pumping rate of 6 L/s and attains an ultimate vacuum pressure of 0.08 MPa. Fig. 4 shows the completed apparatus post-actual fabrication.

3.2. Test method of dynamic water scouring cycle

Three distinct deicing salt solutions—15 % CH_4N_2O, 20 % NaCl, and 20 % CH_2CH_3OH—were individually prepared to serve as the solution for the dynamic water scouring cycle. Marshall specimens of AC-13 and AC-16 were then prepared for the dynamic water scouring cycle examination. The complete dynamic water scouring cycle procedure unfolds

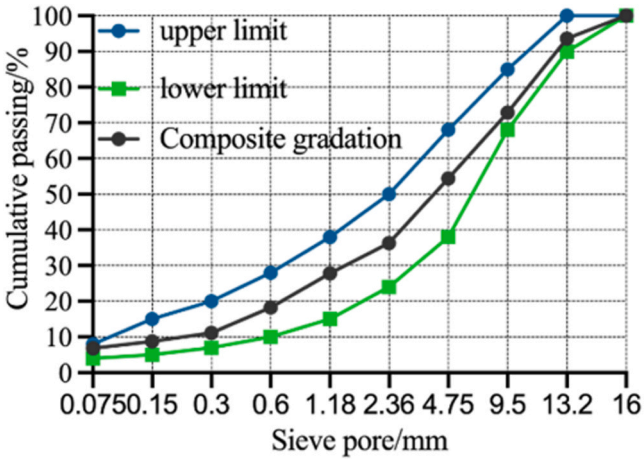

Fig. 1. Aggregate gradation curve of AC-13.

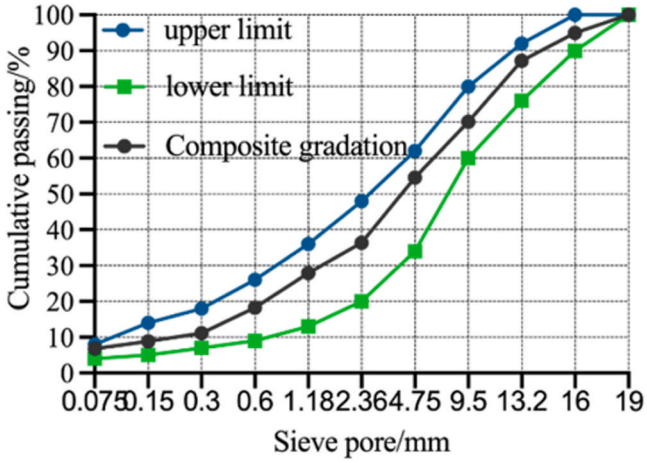

Fig. 2. Aggregate gradation curve of AC-16.

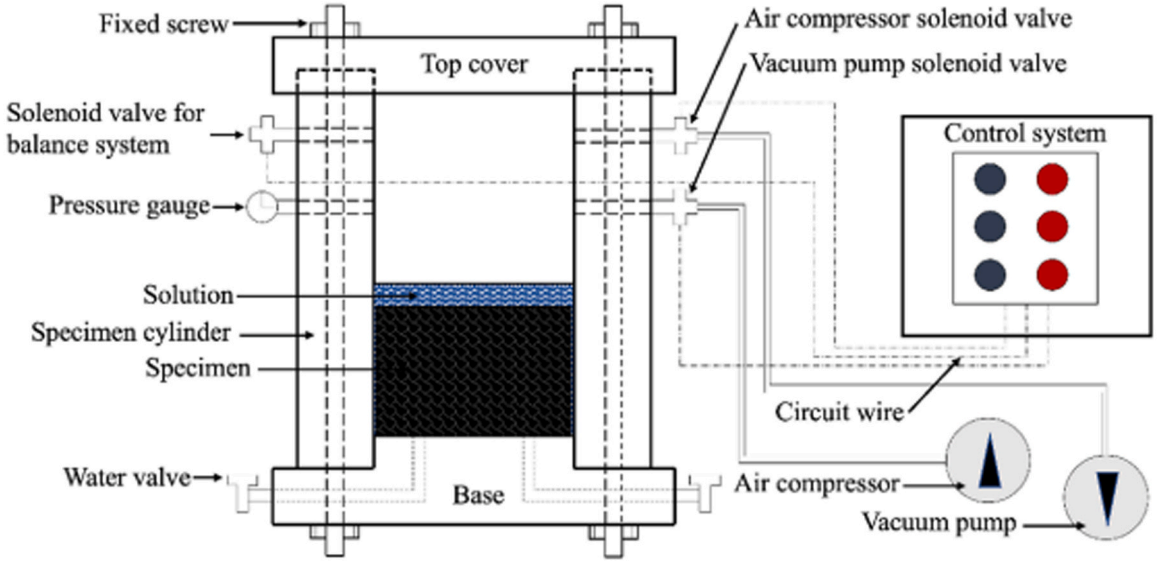

Fig. 3. Schematic diagram of dynamic water scouring simulation apparatus.

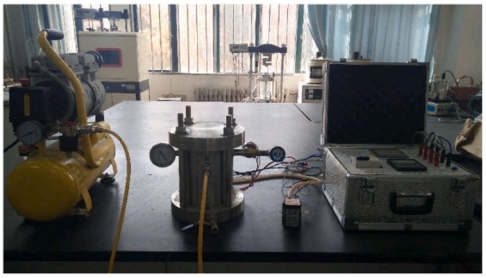

Fig. 4. Dynamic water scouring simulation apparatus post actual fabrication.

as follows:

1. Position a specimen within the pressure simulation container, introduce the prepared deicing salt solution until the solution level surpasses the specimen height by 2–3 mm, and subsequently cover and seal the container.
2. Configure the simulation counts in the control system, followed by activating the switch to commence the scouring cycle operation.
3. Upon completion of the preconfigured cycle count, the apparatus will automatically cease function. Subsequently, extract the specimen, discard the deicing salt solution, and cleanse the container.

The outlined procedure constitutes a full dynamic water scouring cycle. The maximum number of scouring cycles in this examination is 9000, with relevant indicators evaluated after 0, 1000, 2000, 3000, 4000, 5000, 6000, 7000, 8000, and 9000 cycles. The evaluations include the void content test, Marshall water immersion test, and freeze-thaw splitting test. The simulated pressure parameters employed in this study are as follows: positive pressure for 3 s, negative vacuum for 3 s, interval between each positive and negative pressure alternation of 1 s, and interval between each single cycle of 1 s. The dynamic water pressure within the pressure vessel operated within a range of 0.4–0.6 MPa for positive pressure and 0.06–0.08 MPa for negative vacuum pressure.

3.3. Damage analysis based on gray theory

The GM (1,N) model outlines a framework that uses a first-order differential equation to formulate an n-dimensional time series. The foundational theoretical analysis is as follows:

Considering the multifactorial influences on the system, we denote the characteristic data series as:

$$X_1^{(0)} = \left(x_1^{(0)}(1), x_1^{(0)}(2), \ldots, x_1^{(0)}(n)\right) \tag{1}$$

With corresponding factor series defined as:

$$\left\{\begin{array}{l} X_2^{(0)} = \left(x_2^{(0)}(1), x_2^{(0)}(2), \ldots, x_2^{(0)}(n)\right) \\ X_3^{(0)} = \left(x_3^{(0)}(1), x_3^{(0)}(2), \ldots, x_3^{(0)}(n)\right) \\ \cdots \\ X_N^{(0)} = \left(x_N^{(0)}(1), x_N^{(0)}(2), \ldots, x_N^{(0)}(n)\right) \end{array}\right\} \tag{2}$$

The characteristic data series $X_i^{(0)}$ undergoes a single aggregation operation to produce the 1-AGO series $X_i^{(1)}$, $i = 1,2,\ldots N$. Assuming $Z_1^{(1)}$ as the generated sequence of adjacent means of $X_1^{(1)}$, the GM(1,N) gray differential equation is formulated as:

$$x_1^{(0)}(k) + az_1^{(1)}(k) = \sum_{i=2}^{N} b_i x_i^{(1)}(k) \tag{3}$$

Suppose the parameter column of the gray differential equation is $\hat{\boldsymbol{a}} = [a, b_1, b_2, \cdots b_N]^{\mathrm{T}}$, then according to the least squares method:

$$\hat{a} = \left(B^{\mathrm{T}}B\right)^{-1}B^{\mathrm{T}}Y \tag{4}$$

where

$$B = \begin{bmatrix} -z_1^{(1)}(2) & x_2^{(1)}(2) & \cdots & x_N^{(1)}(2) \\ -z_1^{(1)}(3) & x_2^{(1)}(3) & \cdots & x_N^{(1)}(3) \\ \vdots & \vdots & \ddots & \vdots \\ -z_1^{(1)}(n) & x_2^{(1)}(n) & \cdots & x_N^{(1)}(n) \end{bmatrix}, \boldsymbol{Y} = \begin{bmatrix} x_1^{(0)}(2) \\ x_1^{(0)}(3) \\ \vdots \\ x_1^{(0)}(n) \end{bmatrix} \tag{5}$$

The whitening equation of Eq. (3) is then expressed as:

$$\frac{\mathrm{d}x^{(1)}}{\mathrm{d}t} + ax_1^{(1)} = b_2x_2^{(1)} + b_3x_3^{(1)} + \cdots + b_Nx_N^{(1)} \tag{6}$$

Solving the whitening equation yields Eq. (7).

$$x^{(1)}(t) = e^{-at}\left[\sum_{i=2}^{N}\int b_i x_i^{(1)}(t)e^{at}\mathrm{d}t + x^{(1)}(0) - \sum_{i=2}^{N}\int b_i x_i^{(1)}(0)\mathrm{d}t\right] = e^{-at}\left[x_1^{(1)}(0) - t\sum_{i=2}^{N}\int b_i x_i^{(1)}(0) + \sum_{i=2}^{N}\int b_i x_i^{(1)}(t)e^{at}\mathrm{d}t\right] \quad (7)$$

Assuming slight variations in $X_i^{(1)}(i = 1,2,...N)$, $\sum_{i=2}^{N} b_i x_i^{(1)}(k)$ can be approximated as a gray constant. The approximate time response of Eq. (3) is consequently:

$$\hat{x}_1^{(1)}(k+1) = \left[x_1^{(1)}(0) - \frac{1}{a}\sum_{i=2}^{N} b_i x_i^{(1)}(k+1)\right]e^{-ak} + \frac{1}{a}\sum_{i=2}^{N} b_i x_i^{(1)}(k+1) \quad (8)$$

Setting $X_1^{(1)}(0)$ as $X_1^{(1)}(1)$, it results in:

$$\hat{x}_1^{(0)}(k+1) = a^{(1)}\hat{x}_1^{(1)}(k+1) = \hat{x}_1^{(1)}(k+1) - \hat{x}_1^{(1)}(k) \quad (9)$$

4. Analysis and discussion

4.1. Results of air void content and analysis of damage process

The air void content of asphalt mixtures is a critical factor influencing roadway performance. Table 5 presents the experimental results related to the air void content of two different asphalt mixtures, subjected to the concurrent effects of three distinct deicing salts and dynamic water scouring. The variation in the growth rate of air void content for these asphalt mixtures, under the combined influence of three distinct deicing salts and dynamic water scouring, is illustrated in Fig. 5.

As indicated in Table 5, both asphalt mixtures displayed an increasing trend in air void content after exposure to multiple instances of dynamic water scouring. Despite the initially low air void content in both AC-13 and AC-16, the post-scouring variations in air void content were significant—approximately 47 % for AC-13 % and 62 % for AC-16—highlighting the effectiveness of the dynamic water scouring process.

Among the three evaluated deicing salts, CH_4N_2O exerts the most significant influence on air void content, followed by NaCl, with CH_2CH_3OH demonstrating the least impact. The growth rate of air void content in AC-16 is notably higher compared to AC-13. Cooley et al.[24] posit that an air void content ranging from 8% to 12% in asphalt mixtures induces a substantial increase in permeability, thereby amplifying the impact of dynamic water scouring. Despite the peak air void content not exceeding 7.5 % after 9000 iterations of dynamic water scouring, the standard air void content in real-world road construction endeavors often surpasses that of laboratory-compacted specimens. This observation suggests that the cumulative effect of deicing salts and vehicular burden could lead to further deterioration of the mixture's performance.

As shown in Fig. 5, despite AC-16 exhibiting a higher growth rate of air void content than AC-13, two distinct "peaks" emerge in the progression curves of both Fig. 5(a) and Fig. 5(b), indicating a non-uniform progression in air void content. During the initial phase (0–2000 cycles for AC-13; 0–3000 cycles for AC-16), referred to as the micro-crack expansion stage, existing research suggests that during the hydraulic scour erosion process, isolated voids tend to open progressively[25]. Consequently, in this phase, dynamic water erosion triggers the gradual opening of isolated voids, leading to the formation of numerous micro-cracks in the thinner asphalt film adjacent to the surface of the asphalt blend. This process results in the creation of new open pores and initiates a rapid increase in air void content.

The subsequent phase (2000–5000 cycles for AC-13; 3000–5000 cycles for AC-16), termed the pore interconnection phase, involves the introduction of deicing salts into the micro-cracks of the asphalt mixture during ongoing dynamic water scouring. Data indicates that the introduction of these salts causes degradation of the voids within the asphalt mixture[12,26]. In this phase, the erosion caused by deicing salts damages the asphalt film without significantly generating new open voids, resulting in a slower progression of the void ratio.

The third phase (5000–7000 cycles) is the micro-fracture development phase, where the combined impact of deicing salt erosion and dynamic water scouring leads to a substantial increase in new open pores. The rate of air void content increase during this phase surpasses

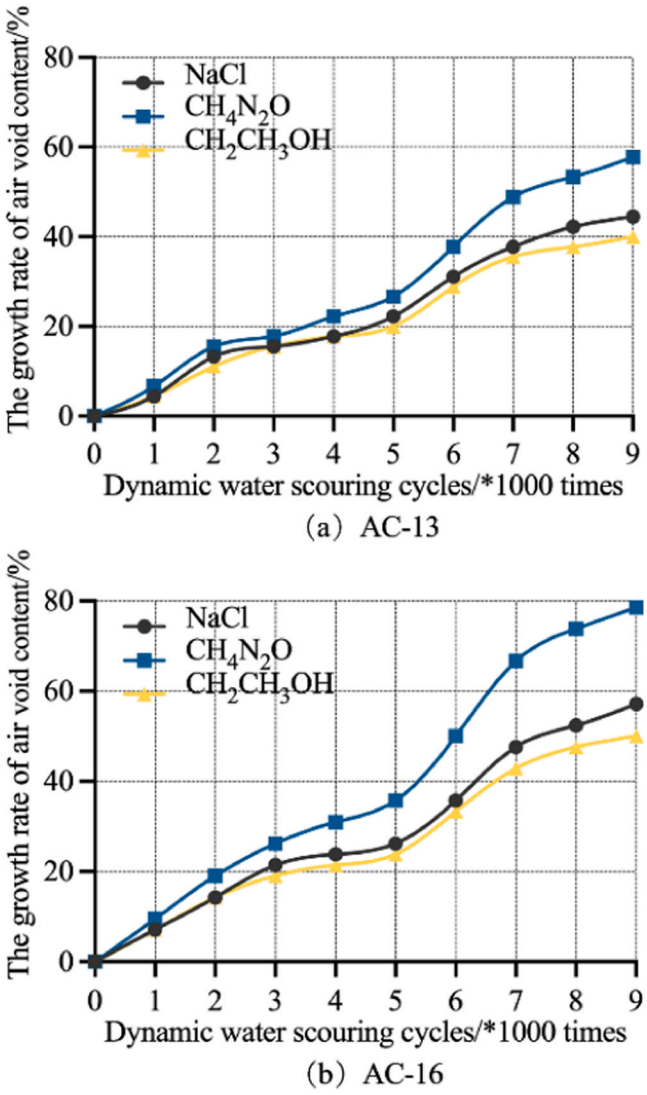

Fig. 5. Growth rate of air void content after multiple dynamic water scouring cycles.

Table 5
Air void content of asphalt mixture after multiple dynamic water scouring cycles.

Scouring times	Air void content/%					
	AC-13			AC-16		
	NaCl	CH_4N_2O	CH_2CH_3OH	NaCl	CH_4N_2O	CH_2CH_3OH
0	4.5	4.5	4.5	4.2	4.2	4.2
1000	4.7	4.8	4.7	4.5	4.6	4.5
2000	5.1	5.2	5	4.8	5	4.8
3000	5.2	5.3	5.2	5.1	5.3	5
4000	5.3	5.5	5.3	5.2	5.5	5.1
5000	5.5	5.7	5.4	5.3	5.7	5.2
6000	5.9	6.2	5.8	5.7	6.3	5.6
7000	6.2	6.7	6.1	6.2	7	6
8000	6.4	6.9	6.2	6.4	7.3	6.2
9000	6.5	7.1	6.3	6.6	7.5	6.3

that of the first phase. Finally, the last stage (7000–9000 cycles) returns to the pore interconnection phase. At this point, the thin asphalt film has predominantly achieved interconnectivity, yet some asphalt films are still gradually deteriorating under the combined impact of deicing salt and dynamic water erosion, leading to the formation of new open pores, albeit in fewer numbers.

4.2. Results of water stability and analysis of damage process

The present study examines the damage patterns of asphalt mixture water stability under the simultaneous influence of deicing salts and dynamic water scouring, utilizing both the Marshall water immersion test and the freeze-thaw splitting test. The results from the residual stability assessments of two asphalt mixture types under the combined effects of three categories of deicing salts and dynamic water scouring are presented in Table 6. Additionally, Table 7 provides details on the Tensile Strength Ratio (TSR) of the two asphalt mixture types under identical conditions. The variations in the loss rate of residual stability for both asphalt mixture types under the combined influence of the three deicing salt types and dynamic water scouring are illustrated in Fig. 6, while Fig. 7 depicts the changes in the TSR loss rate under analogous conditions.

Table 6 illustrates a discernible declining trend in the residual stability of both asphalt mixture categories with an increase in the number of dynamic water scouring cycles. Among the trio of deicing salts, CH_4N_2O has the most pronounced impact on residual stability, followed by NaCl, while CH_2CH_3OH induces the least effect. According to prevailing standards, residual stability should surpass 75 %. However, with the AC-13 asphalt mixture, the residual stability under CH_4N_2O's influence registers at 73.8 % at the 3000th cycle, 74.9 % under NaCl's influence at the 4000th cycle, and 74.5 % under CH_2CH_3OH's impact at the 7000th cycle, all falling short of the required standards. Similarly, with the AC-16 asphalt mixture, the residual stability stands at 74.1 % under CH_4N_2O's influence at the 2000th cycle, 73.8 % under NaCl at the 4000th cycle, and 73.7 % under CH_2CH_3OH at the 6000th cycle, none of which meet the stipulated standards.

Table 7 shows that as the number of dynamic water scouring cycles increases, the TSR for both asphalt mixtures tends to decrease. The impact of the three types of deicing salts on TSR follows this ranking: CH_4N_2O > NaCl > CH_2CH_3OH. The rate of decline in TSR for AC-16 significantly exceeds that of AC-13. According to current standards, the TSR should be above 70 %. For the AC-13 asphalt mixture, TSR under the influence of CH_4N_2O is 69.1 % at the 3000th cycle, 68.4 % under NaCl at the 4000th cycle, and 69.5 % under CH_2CH_3OH at the 5000th cycle, all falling short of the specified mandates. Similarly, for the AC-16 asphalt mixture, TSR is 69.7 % at the 2000th cycle under CH_4N_2O, 69.0 % at the 4000th cycle under NaCl, and 69.1 % at the 6000th cycle under CH_2CH_3OH, all of which also fail to meet the specified requirements.

Table 6
Residual stability of asphalt mixture after multiple dynamic water scouring cycles.

Scouring times	Residual stability/%					
	AC-13			AC-16		
	NaCl	CH_4N_2O	CH_2CH_3OH	NaCl	CH_4N_2O	CH_2CH_3OH
0	86.8	86.8	86.8	85.0	85.0	85.0
1000	83.8	82.5	84.5	79.8	78.4	81.5
2000	80.0	77.9	82.3	75.7	74.1	76.0
3000	75.8	73.8	78.6	75.1	70.6	75.6
4000	74.9	70.6	76.8	73.8	69.1	75.4
5000	73.8	68.8	75.8	71.5	66.9	75.2
6000	73.3	67.1	75.2	70.8	66.0	73.7
7000	72.8	65.9	74.5	65.9	60.4	70.4
8000	68.0	61.2	70.3	63.4	56.1	67.3
9000	61.3	55.5	65.1	58.6	51.9	62.3

Table 7
TSR of asphalt mixture after multiple dynamic water scouring cycles.

Scouring times	TSR/%					
	AC-13			AC-16		
	NaCl	CH_4N_2O	CH_2CH_3OH	NaCl	CH_4N_2O	CH_2CH_3OH
0	75.9	75.9	75.9	79.8	79.8	79.8
1000	74.3	73.4	75.0	73.8	72.8	74.7
2000	71.8	71.0	72.8	71.0	69.7	71.2
3000	70.1	69.1	71.3	70.1	68.0	70.5
4000	68.4	67.1	70.1	69.0	67.4	70.3
5000	68.1	66.6	69.5	67.8	65.4	70.0
6000	67.8	66.2	69.2	67.4	64.8	69.1
7000	67.3	65.3	69.1	64.6	61.9	66.9
8000	65.7	61.9	67.2	62.6	58.9	65.4
9000	63.7	59.0	65.1	60.4	55.7	63.9

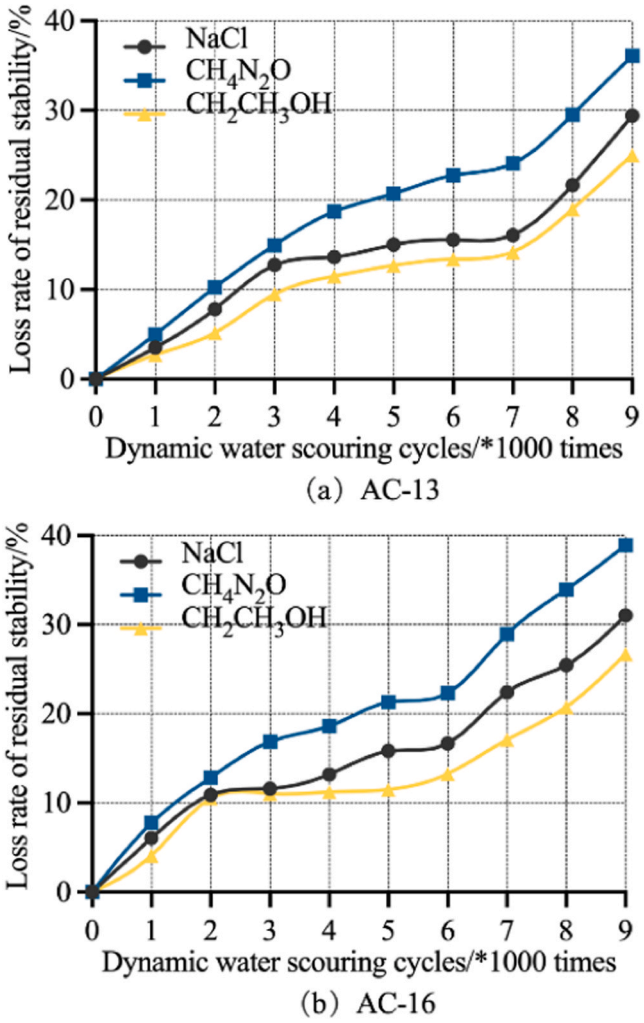

Fig. 6. Loss rate of residual stability after multiple dynamic water scouring cycles.

Based on the quantitative analysis of air void content, residual stability, and TSR, it is evident that among the three deicing salt solutions, CH_4N_2O exerts the most significant impact on water stability, likely due to its chemical properties inducing enhanced erosion[27]. NaCl follows, exerting a moderate influence on water stability. According to Zhen's research[28], chloride salts contribute to the formation of an unstable, water-soluble amorphous film on the asphalt surface, encapsulating the honeycomb structure, thereby undermining the mixture and diminishing water stability. In contrast, CH_2CH_3OH has a comparatively lesser

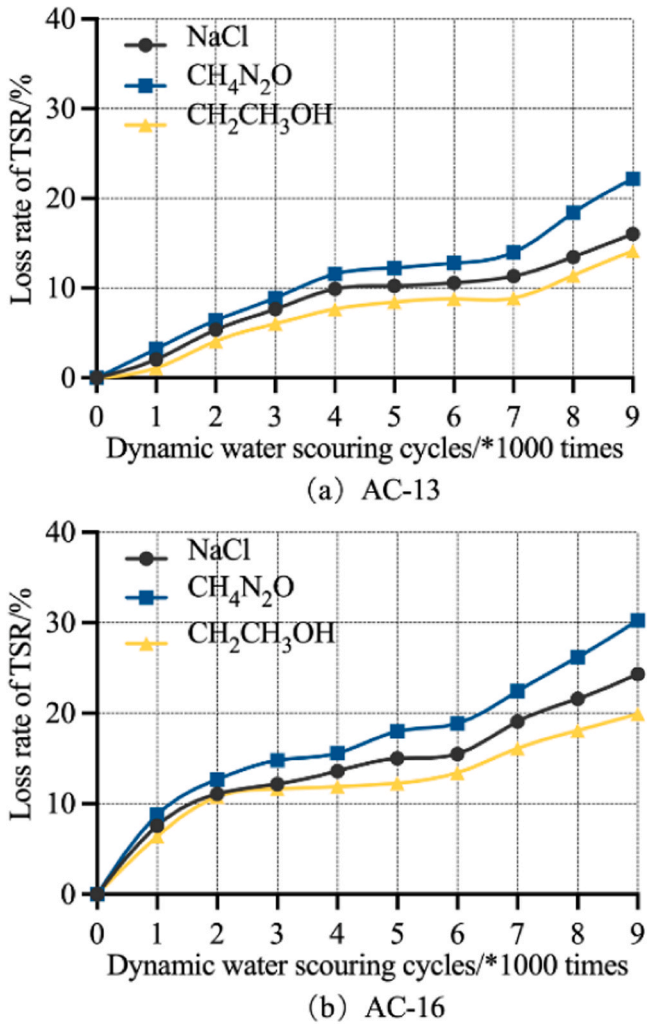

Fig. 7. Loss rate of TSR after multiple dynamic water scouring cycles.

impact. Literature suggests that the chemical interaction and diffusion between alcohol and asphalt binder contribute to the structural degradation of the asphalt mixture[29], accounting for the observed reduction in water stability. Additionally, the rate of decline in water stability for AC-16 is markedly swifter than that for AC-13. This differential is potentially linked to the compositional characteristics of the two asphalt mixtures. AC-13 has a higher percentage of fine aggregate compared to AC-16, and the findings indicate that asphalt mixture stripping is predominantly influenced by the fine aggregate rather than the coarse aggregate[30,31], thereby elucidating the observed trend.

Figs. 6 and 7 depict graphs for the two types of asphalt mixtures and the three deicing salts, revealing a pattern of initial rapid growth, intermediate slow progression, and eventual brisk rise. Based on these observations, the water damage of asphalt mixtures can be divided into three distinct phases: the accelerated damage phase, damage propagation phase, and damage intensification phase. In the initial accelerated damage phase, the water-induced harm to the specimen is mainly attributed to the dynamic water-scouring process. Following Kandhal's research, the physical degradation of asphalt mixtures is linked to the rapid water flow within the mixture's voids during the diffusion phase [32]. During this phase, aggregates prone to detachment from the specimen's external part initiate detachment, and micro-cracks begin interconnecting under dynamic water pressure impact, thereby developing progressively and inducing a sharp increase in water damage. In the subsequent damage propagation phase, the water-induced harm to the specimen predominantly stems from the erosive action of deicing salts. Erosion stemming from salt solutions infiltrating the voids and fissures of asphalt mixtures is widely recognized as a contributory element in the degradation of such mixtures[17]. Micro-cracks undergo gradual development under the influence of dynamic water pressure, allowing deicing salts to penetrate voids and induce erosive damage. This gradual process weakens the bond between the asphalt layer and aggregate, resulting in a slower escalation of water damage. In the final phase of the damage intensification, deicing salts erode the bond strength between asphalt and aggregate, leading to significant micro-crack infiltration. Dynamic water pressure continues to impact the asphalt and aggregate, causing aggregate peeling and the most rapid increase in water damage.

4.3. Prediction model of air void content

Based on the experimental results concerning air void content, GM(1, N) prediction models were constructed using the gray theory. These models were then applied to predict the air void content of the asphalt mixtures after 0–12,000 cycles of dynamic water scouring. A comparison between the projected air void content values and the actual experimental measurements is illustrated in Fig. 8. The relative discrepancy between the forecasted outcomes and the experimental findings for the established model remains within a 5% range, eliminating the need for further adjustments. The results of the prediction models are presented in Table 8.

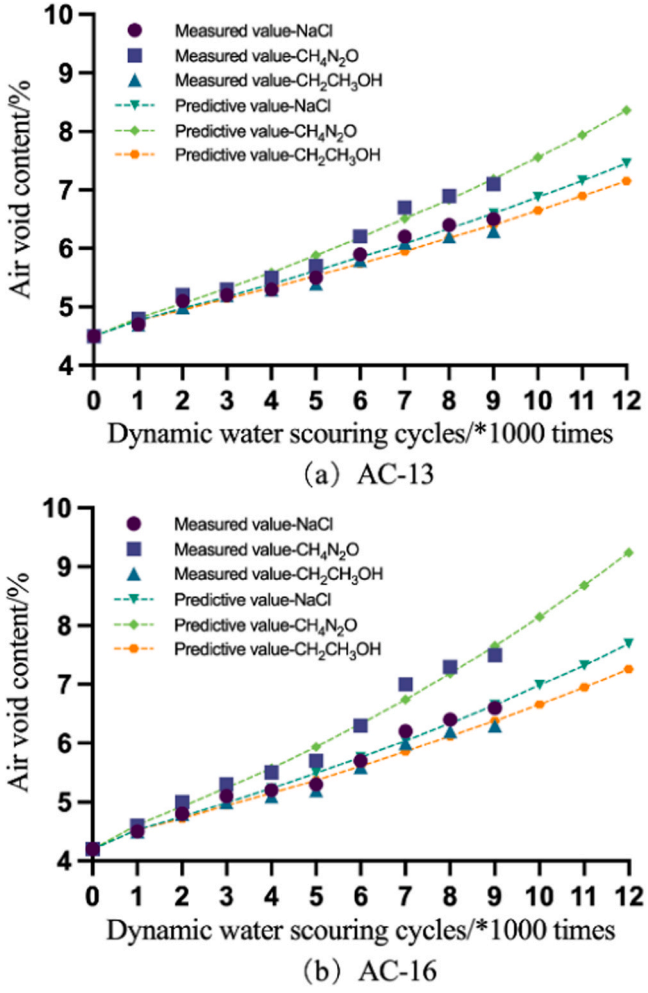

Fig. 8. Comparison of predicted and experimentally measured values of air void content.

Table 8
Outcomes of air void content prediction models employing GM(1, N).

Prediction model		
AC-13	NaCl	$\hat{x}^{(1)}(k+1) = 115.5173e^{0.0405k} - 111.0173$
	CH_4N_2O	$\hat{x}^{(1)}(k+1) = 93.4442e^{0.0502k} - 88.9442$
	CH_2CH_3OH	$\hat{x}^{(1)}(k+1) = 127.32882e^{0.0368k} - 122.8288$
AC-16	NaCl	$\hat{x}^{(1)}(k+1) = 91.9006e^{0.0481k} - 87.7006$
	CH_4N_2O	$\hat{x}^{(1)}(k+1) = 70.7253e^{0.0632k} - 66.5253$
	CH_2CH_3OH	$\hat{x}^{(1)}(k+1) = 103.2979e^{0.0429k} - 99.0979$

Table 9
Outcomes of residual stability prediction models employing GM (1, N).

Prediction model		
AC-13	NaCl	$\hat{x}^{(1)}(k+1) = -2804.5267e^{-0.03k} + 2891.3267$
	CH_4N_2O	$\hat{x}^{(1)}(k+1) = -1957.3080e^{-0.0426k} + 2044.1080$
	CH_2CH_3OH	$\hat{x}^{(1)}(k+1) = -3177.5532e^{-0.0269k} + 3264.3532$
AC-16	NaCl	$\hat{x}^{(1)}(k+1) = -2451.1562e^{-0.0333k} + 2536.1562$
	CH_4N_2O	$\hat{x}^{(1)}(k+1) = -1756.8996e^{-0.0458k} + 1841.8996$
	CH_2CH_3OH	$\hat{x}^{(1)}(k+1) = -3161.2780e^{-0.0259k} + 3246.2780$

4.4. Prediction model of residual stability

Based on the experimental outcomes related to residual stability, a series of GM (1,N) prediction models were developed using the gray theory. These models were then utilized to predict the residual stability of the asphalt mixtures after 0–12,000 cycles of dynamic water scouring. Fig. 9 illustrates a comparison between the projected residual stability values and the actual experimental determinations. The relative deviation between the forecasted results and the experimental data for the developed models remains within a 5 % boundary, eliminating the need for residual corrections. The results of the prediction models are presented in Table 9.

4.5. Prediction Model of TSR

Building upon the experimental findings related to TSR, several GM (1,N) prediction models were formulated using the gray theory. These models were then employed to predict the TSR of the asphalt mixtures after 0–12,000 cycles of dynamic water scouring. A comparative analysis between the predicted TSR values and the actual experimental measurements is illustrated in Fig. 10. The relative deviation between the anticipated outcomes and the experimental test results for the formulated models remains within a 5 % limit, eliminating the need for residual adjustment. The results of the prediction models are outlined in Table 10.

5. Conclusion and recommendations

This study investigates the collective impact of three deicing salts

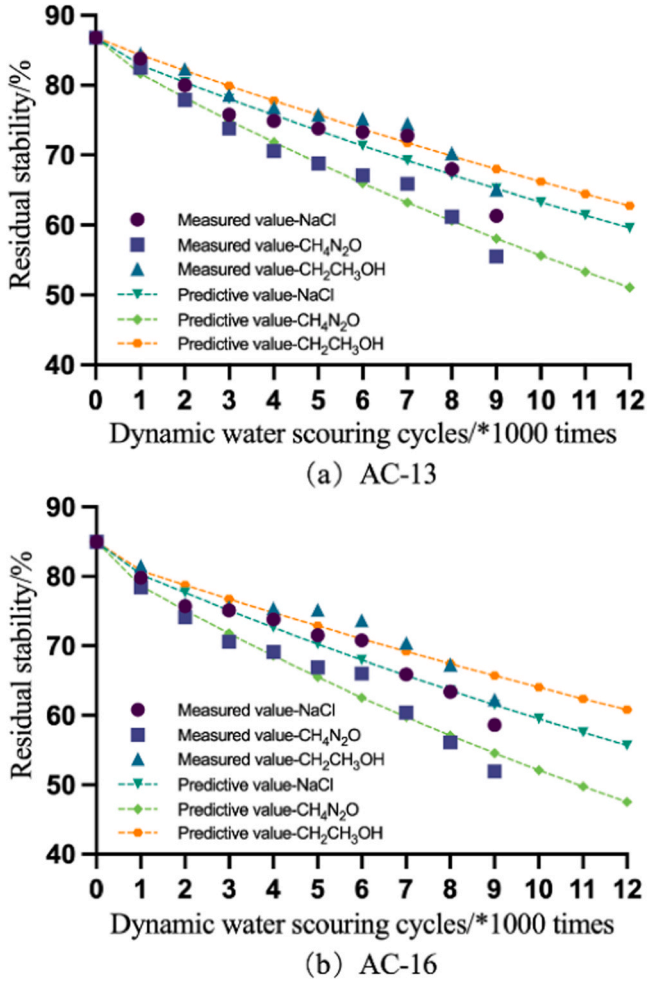

Fig. 9. Comparison of predicted and experimentally measured values of residual stability.

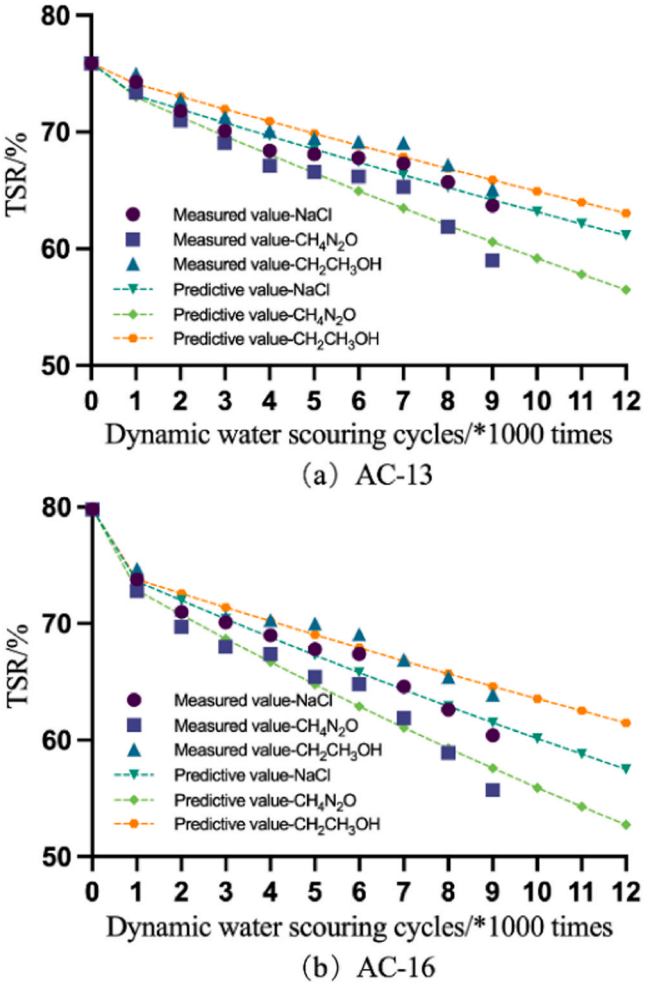

Fig. 10. Comparison of predicted and experimentally measured values of TSR.

Table 10
Outcomes of TSR prediction models employing GM (1, N).

Prediction model		
AC-13	NaCl	$\hat{x}^{(1)}(k+1) = -4523.7564e^{-0.0163k} + 4599.6564$
	CH_4N_2O	$\hat{x}^{(1)}(k+1) = -3169.2288e^{-0.0233k} + 3245.1288$
	CH_2CH_3OH	$\hat{x}^{(1)}(k+1) = -5078.9027e^{-0.0147k} + 5154.8027$
AC-16	NaCl	$\hat{x}^{(1)}(k+1) = -3309.1067e^{-0.0225k} + 3388.9067$
	CH_4N_2O	$\hat{x}^{(1)}(k+1) = -2514.3871e^{-0.0294k} + 2594.1871$
	CH_2CH_3OH	$\hat{x}^{(1)}(k+1) = -4481.8024e^{-0.0166k} + 4561.6024$

and dynamic water scouring cycles on the short-term water damage of two asphalt mixtures. The evaluation is based on changes in air void content, residual stability, and TSR. Employing gray theory, the data was modeled and predicted, leading to the following conclusions:

(1) The conjunction of salt corrosion and dynamic water scouring significantly influences the short-term performance alterations of asphalt mixtures. By the end of the experiment, the air void content verges on the non-recommended threshold; concurrently, water stability indicators under varied deicing salts descend beneath the minimum values delineated by standards, predominantly during the initial or mid-to-late phases of dynamic water scouring.
(2) Data analysis indicates that dynamic water scouring plays a key role in the initial stages of water damage to asphalt mixtures, causing the "physical" degradation of the binder-aggregate bonds, promoting microcracks, and triggering aggregate shedding. The intermediate phase is predominantly influenced by corrosion induced by deicing salts, resulting in the "chemical" impairment of the binder. In the final phase, after deicing salts corrosion, dynamic water scouring continues against a backdrop of diminished binder-aggregate adhesion, leading to more pronounced damage.
(3) The evaluation of the influence of the three deicing salts shows that CH_4N_2O has the most substantial impact on the short-term water damage of asphalt mixtures, likely owing to its chemical composition conducive to enhanced erosion, succeeded by NaCl, while CH_2CH_3OH leaves the least imprint. Evaluating the experimental data for both asphalt mixtures reveals that AC-13 demonstrates superior resistance to water-induced degradation under the combined influence of deicing salts and dynamic water scouring compared to AC-16. This resistance can be attributed to the fact that asphalt mixture stripping is predominantly influenced by the fine aggregate; thus, augmenting the proportion of fine aggregate in the mixture bolsters its water damage resistance.
(4) Employing Gray Theory's GM(1,N) model to analyze and assess short-term water damage in asphalt mixtures produced prediction outcomes with a relative error below 5% when compared to the experimental results. This capacity to predict the experimental data offers robust theoretical and technical support for assessing and forecasting asphalt mixture performance in cold regions.

CRediT authorship contribution statement

Kovalskiy Viktor Pavlovich: Visualization, Validation, Supervision, Resources. **Li Ping:** Visualization, Validation, Supervision, Project administration. **Nian Tengfei:** Writing – review & editing, Writing – original draft, Project administration, Methodology, Investigation, Formal analysis, Data curation, Conceptualization. **Guo Mingjun:** Writing – review & editing, Writing – original draft, Software, Resources, Methodology, Investigation, Funding acquisition, Formal analysis, Data curation.

Declaration of Competing Interest

The authors declared there are no conflicts of interest.

Data availability

No data was used for the research described in the article.

Acknowledgments

This work was financial supported by the National Natural Science Foundation of China (No.: 52368066), Lanzhou University of Technology Hongliu Outstanding Young Talent Program, China (No.: 04–062005), Natural Science Foundation of Gansu Province, China (No.: 23JRRA773), Gansu Provincial University Innovation Fund Project (No.: 2022A-026), and the China Scholarship Council (No.: 201905650001).

References

[1] M. Gong, H. Zhang, Z. Liu, X. Fu, Study on PQI standard for comprehensive maintenance of asphalt pavement based on full-cycle, Int. J. Pavement Eng. 23 (2022) 4277–4290.
[2] L. Yao, Z. Leng, J. Jiang, F. Ni, Large-scale maintenance and rehabilitation optimization for multi-lane highway asphalt pavement: a reinforcement learning approach, IEEE Trans. Intell. Transp. Syst. 23 (2022) 22094–22105.
[3] H. Wu, P. Li, T. Nian, G. Zhang, T. He, X. Wei, Evaluation of asphalt and asphalt mixtures' water stability method under multiple freeze-thaw cycles, Constr. Build. Mater. 228 (2019), 117089, https://doi.org/10.1016/j.conbuildmat.2019.117089.
[4] P. Zhao, H. Zhang, B. Ma, C. Duojie, W. Si, Y. Hu, Influence of subgrade freezing and thawing on vertical deformation of asphalt pavement, J. Test. Eval. 50 (2022) 2116–2136.
[5] T. Ma, D. Zhang, Y. Zhang, Y. Zhao, X. Huang, Effect of air voids on the high-temperature creep behavior of asphalt mixture based on three-dimensional discrete element modeling, Mater. Des. 89 (2016) 304–313.
[6] A.G. Veith, Tire wet traction performance: the influence of tread pattern, Transp. Res. Rec. 621 (1977) 113–125.
[7] Gao Junqi, Sheng Yuxiang, Zhang Shiduo, Yu Fengqiang, Jiang Zemin, Analysis on infiltration capacity in asphalt pavement subjected to dynamic hydraulic pressure, J. Nanjing Univ. Aeronaut. Astronaut 45 (2013) 266–270.
[8] Zhang Yan, Gu Xingyu, Xing Shiqin, Wang Xiaowei, Cui Bingyan, Study on dynamic water pressure of asphalt pavement structure based on COMSOL fluid-solid coupling, Munic. Eng. Technol. 38 (2020) 48–52+64.
[9] Li Atan, Yu Jiangmiao, Wang Gang, Wang Xiaoxiao, Research on water damage evaluation of asphalt pavement based on dynamic water scouring, Test., Highw. 61 (2016) 58–63.
[10] Guo Xuedong, Li Zhun, Ma Guirong, Li Yingsong, Wang Zhenyong, Guo Wei, Li Jilu, Analysis of factors affecting water-damage of asphalt mixture under hydrodynamic pressure, Highway 64 (2019) 21–27.
[11] F. Wang, X. Qin, W. Pang, W. Wang, Performance deterioration of asphalt mixture under chloride salt erosion, Materials 14 (2021) 3339.
[12] K. Zhang, W. Li, F. Han, Performance deterioration mechanism and improvement techniques of asphalt mixture in salty and humid environment, Constr. Build. Mater. 208 (2019) 749–757.
[13] Y. Zhang, Z. Liu, X. Shi, Development and use of salt-storage additives in asphalt pavement for anti-icing: literature review, J. Transp. Eng. Part B Pavements 147 (2021), 03121002.
[14] E. Yang, J. Peng, L. Luo, H. Zhang, H. Di, F. Yuan, Y. Qiu, Analysis on influencing factors of asphalt pavement icing and establishment of icing prediction model, Road. Mater. Pavement Des. (2023) 1–17.
[15] B. Feng, H. Wang, S. Li, K. Ji, L. Li, R. Xiong, The durability of asphalt mixture with the action of salt erosion: a review, Constr. Build. Mater. 315 (2022), 125749.
[16] R. Xiong, C. Chu, B. Guan, Y. Sheng, Performance damage characteristics of asphalt mixture suffered from the sulphate–water–temperature–load coupling action, Int. J. Pavement Eng. 23 (2022) 1368–1377.
[17] R. Xiong, C. Chu, N. Qiao, L. Wang, F. Yang, Y. Sheng, B. Guan, D. Niu, J. Geng, H. Chen, Performance evaluation of asphalt mixture exposed to dynamic water and chlorine salt erosion, Constr. Build. Mater. 201 (2019) 121–126.
[18] A.J. Enríquez-León, T.D. de Souza, F.T.S. Aragão, A.M.B. Pereira, L.P. Nogueira, Characterization of the air void content of fine aggregate matrices within asphalt concrete mixtures, Constr. Build. Mater. 300 (2021), 124214.
[19] M. Guo, V.P. Kovalskiy, T. Nian, P. Li, Influence of deicer on water stability of asphalt mixture under freeze–Thaw cycle, Sustainability 15 (2023) 13707.
[20] D. Julong, Introduction to grey system theory, J. Grey Syst. 1 (1989) 1–24.
[21] B. Zeng, M. Tong, X. Ma, A new-structure grey Verhulst model: development and performance comparison, Appl. Math. Model. 81 (2020) 522–537.
[22] H. Zhu, Multi-parameter grey prediction model based on the derivation method, Appl. Math. Model. 97 (2021) 588–601.
[23] Yang liu, Ping Li, Study on Temperature Field Prediction Model and Anti Icing Technology of Asphalt Pavement in Winter of Gansu Province, Master, Lanzhou University of Technology,, 2018.

[24] L.A. Cooley, B.D. Prowell, E. Brown, Issues pertaining to the permeability characteristics of coarsegraded superpave mixes, 2002.
[25] H. Xu, F. Chen, X. Yao, Y. Tan, Micro-scale moisture distribution and hydrologically active pores in partially saturated asphalt mixtures by X-ray computed tomography, Constr. Build. Mater. 160 (2018) 653–667.
[26] K. Zhang, Y. Luo, Z. Li, Y. Zhao, Y. Zhao, Evaluation of performance deterioration characteristics of asphalt mixture in corrosion environment formed by snow-melting agents, J. Mater. Civ. Eng. 34 (2022), 04021481.
[27] A. Galakhova, F. Kadisch, G. Mori, S. Heyder, H. Wieser, B. Sartory, S. Burger, Corrosion of stainless steel by urea at high temperature, Corros. Mater. Degrad. 2 (2021) 461–473.
[28] Z. Long, N. Guo, X. Tang, Y. Ding, L. You, F. Xu, Microstructural evolution of asphalt induced by chloride salt erosion, Constr. Build. Mater. 343 (2022), 128056.
[29] A.C. Falchetto, M.I. Turos, M.O. Marasteanu, Investigation on asphalt binder strength at low temperatures, Road. Mater. Pavement Des. 13 (2012) 804–816.
[30] G.W. Maupin Jr, T.H.E. USE, The use of antistripping additives in Virginia (with discussion), in: Assoc. Asph, Paving Technol. Proc., 1982.
[31] T.W. Kennedy, F.L. Roberts, K.W. Lee, Evaluation of moisture susceptibility of asphalt mixtures using the Texas Freeze-Thaw Pedestal Test, in: Assoc. Asph, Paving Technol. Proc., 1982.
[32] P.S. Kandhal, C.W. Lubold, F.L. Roberts, Water damage to asphalt overlays: case histories (with discussion), in: Assoc. Asph, Paving Technol. Proc, 1989.